A thermoporometry and small-angle x-ray scattering study of wet silica sonogels as the pore volume fraction is varied

2008 J. Phys.: Condens. Matter 20 025225

(http://iopscience.iop.org/0953-8984/20/2/025225)

J. Phys.: Condens. Matter **20** (2008) 025225 (7pp) doi:10.1088/0953-8984/20/02/025225

A thermoporometry and small-angle x-ray scattering study of wet silica sonogels as the pore volume fraction is varied

D R Vollet, J P Scalari, D A Donatti and A Ibañez Ruiz

IGCE, Departamento de Física, Unesp—Univerisdade Estadual Paulista, POB 178, CEP 13500-970 Rio Claro (SP), Brazil

E-mail: vollet@rc.unesp.br

Received 4 October 2007, in final form 6 November 2007
Published 13 December 2007
Online at stacks.iop.org/JPhysCM/20/025225

Abstract

Silica sonogels with different porosities were prepared by acid sono-hydrolysis of tetraethoxysilane. Wet sonogels were studied using small-angle x-ray scattering (SAXS) and differential scanning calorimetry (DSC). The DSC shows a broad thermal peak below the normal water melting point associated with the melting of confined ice nanocrystals, or nanoporosity. The nanopore size distribution was determined from the Gibbs–Thomson equation. As the porosity is increased, a second sharp DSC thermal peak with onset temperature at the water melting point is apparent, which was associated with the melting of ice macrocrystals, or macroporosity. The DSC result could be causing misinterpretation of the macroporosity because water may not be exactly confined in very feeble silica network regions in sonogels with high porosity. The structure of the wet gels can be described fairly well as mutually self-similar mass fractal structures with characteristic length ξ increasing from ∼1.8 to ∼5.4 nm and mass fractal dimension D diminishing discretely from ∼2.6 to ∼2.3 as the porosity increases in the range studied. More specifically, such a structure could be described using a two-parameter correlation function $\gamma(r) \sim r^{D-3} \exp(-r/\xi)$, which is limited at larger scale by the cut-off distance ξ but without a well-defined small scale cut-off distance, at least up to the maximum angular domain probed using SAXS in the present study.

1. Introduction

A large variety of glasses and glass ceramics have been obtained by the sol–gel process from the hydrolysis of tetraethoxysilane (TEOS) [1]. Silica gels have been considered as appropriate matrices for the preparation of complex-center doped materials for a variety of metallic ions [2, 3] and for encapsulation of a variety of organic [4–6] and inorganic compounds [7, 8], with interesting optical and/or electronic properties. The mesoporous structure has been considered an important transport medium for a variety of applications such as in controlled-release carrier implantable materials for low weight drugs in biological systems [9, 10] and in substitution materials for membrane processes in fuel cells [11].

Different structures for gels have been reported, depending on the starting materials, the initial conditions of preparation such as pH, alcoxide/water molar ratio, type of catalyst, temperature and method employed for hydrolysis (ultrasound or conventional), and also the conditions of gelation, ageing and drying of the gels. Most of the structural properties of the gels are even defined for the early gelation and ageing period in which the gels are yet to be in wet conditions. Thus the structural parameters of the wet gels are important for purposes of control of the final product. Small-angle x-ray scattering (SAXS) has been successfully applied to study the structure of wet gels (and also of aerogels) due to the non-destructive character of the technique. Nuclear magnetic resonance (NMR) [12, 13], small-angle neutron scattering (SANS) [14], and differential scanning calorimetry (DSC) approaches [15] are also appropriate techniques for studying the structure of wet gels. In particular, DSC is applicable in studying nanopore size distributions in wet gels and it seems to provide evidence of a macroporosity apparently hidden in the observations of other techniques, such as SAXS and nitrogen adsorption approaches [16]. However, the existence of a threshold porosity for the appearing of the macroporosity and

Table 1. Structural properties of the wet gel.

R	V_p (cm^3/g-SiO_2)	ρ (g-SiO_2/cm^3)	V_{macro} (cm^3/g-SiO_2)	A (arb. units)	D	ξ (nm)
4	1.70 ± 0.02	0.46 ± 0.01	0	40.3 ± 0.7	2.58 ± 0.03	1.8 ± 0.1
6	1.93 ± 0.02	0.42 ± 0.01	0.12 ± 0.02	54.4 ± 0.6	2.55 ± 0.03	2.1 ± 0.1
8	2.24 ± 0.02	0.37 ± 0.01	0.17 ± 0.02	75.0 ± 0.8	2.51 ± 0.03	2.5 ± 0.1
12	2.78 ± 0.03	0.309 ± 0.009	0.43 ± 0.03	141 ± 1	2.41 ± 0.03	3.5 ± 0.1
16	3.28 ± 0.03	0.268 ± 0.008	0.85 ± 0.04	278 ± 3	2.32 ± 0.03	5.4 ± 0.1

its effect on the structure of the sonogels are not established completely. In this work, wet sonogels with different 'pore' volume fractions were prepared in order to probe the evolution of both the nanoporosity and the macroporosity by means of DSC thermoporometry. The results were discussed comparing to SAXS data.

2. Experimental procedure

The samples were prepared from the acid sono-hydrolysis of mixtures of tetraethoxysilane (TEOS), distilled and deionized water, and 0.1 N HCl as a catalyst. The hydrolysis water/TEOS molar ratio (R) was changed as $R = 4$, 6, 8, 12 and 16. The hydrolysis was promoted for 10 min under a constant power ($\sim$0.7 W cm^{-3}) of ultrasonic radiation. The pH of the resulting sol was increased to 4.5 by $NH_4(OH)$ addition in order to accelerate the gelation process. The resulting sol was cast in sealed containers and kept under saturated conditions for 30 days at 40 °C for gelation and ageing. The liquid phase of the wet gels, a mixture of ethanol and water, was exchanged with pure water for the DSC tests and SAXS analysis.

The DSC thermograms were obtained with a heating rate of 2 °C min^{-1} in the temperature range from −120 °C up to 30 °C using commercial equipment (DSC 200 Phox Netzsch). The temperature and the sensitivity scales of the DSC equipment were calibrated using the melting point and the enthalpy of fusion of six pure standards with melting points in the range between −86.1 and 474.4 °C.

The SAXS experiments were carried out using synchrotron radiation with a wavelength $\lambda = 0.1608$ nm. The experiments were performed at LNLS—Brazilian Synchrotron Light Laboratory—Brazil. The beam was monochromatized by a silicon monochromator and collimated by a set of slits defining a pinhole geometry [17]. A one-dimensional position sensitive x-ray detector was used to record the SAXS intensity, $I(q)$, as a function of the modulus of the scattering vector $q = (4\pi/\lambda)\sin(\theta/2)$, where θ is the scattering angle. The experimental setup allowed us to get SAXS data from $q_{min} = 0.069$ nm^{-1} to $q_{max} = 3.27$ nm^{-1} with increments of $\Delta q = 2.56 \times 10^{-3}$ nm^{-1}. The data were corrected for the sample attenuation and the parasitic scattering, and normalized with the intensity of the incident beam and the logarithm of the attenuation, which is proportional to the thickness of the sample.

3. Results

Table 1 shows the total 'pore' volume V_p per silica mass unit as determined from thermogravimetric (TG) measurements on the water-exchanged wet gels. As expected, the 'porosity' of the wet gels increases with the hydrolysis water/TEOS molar ratio R. The bulk density ρ of the hypothetical 'aerogel', which would be obtained after complete extraction of the liquid phase of the wet gels, was evaluated (table 1) from the TG data, assuming the value 2.2 g cm^{-3} for the density of the silica particles building up the gel structure.

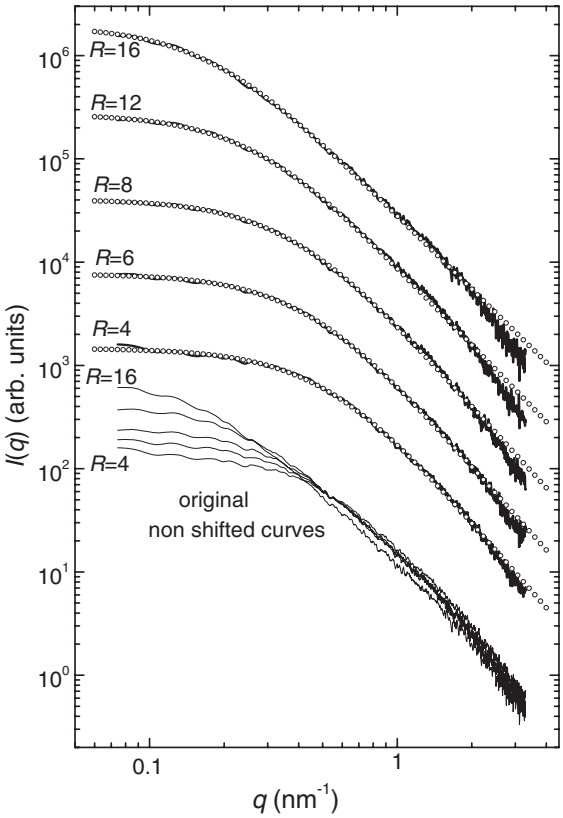

Figure 1. SAXS intensity for the wet gels as a function of the hydrolysis water/TEOS molar ratio R. The curves were drawn once more after shifting vertically by different factors, for the sake of clarity. The small circle lines are fittings of equation (1) to the experimental data.

Figure 1 shows the SAXS intensity $I(q)$ of the wet gels as a function of R. The data were interpreted in terms of a mass fractal approach. Mass fractal structures can be recognized by a typical power law decrease in q for the SAXS intensity as $I(q) \sim q^{-D}$ in a range of q given by $\xi \gg q^{-1} \gg a$, where ξ is the characteristic length and D the mass fractal dimension of the structure (a physically acceptable value when $1 < D < 3$), and a the characteristic length of the primary silica particle building up the mass fractal structure [18].

The SAXS intensity departs from the power law regime at low q, due to the finite correlation length ξ of the mass fractal structure, and at high q, due to the finite characteristic length a of the primary particle building up the structure. The effect of the upper (ξ) and lower (a) cut-offs on the mass fractal-like structures has been treated by Sinha [19] and Teixeira [20]. A simplified approach accounting for the upper cut-off (ξ), which is valid for the low and intermediate q ranges in systems with very small particle size a, has been employed by Vacher *et al* [21]. That can be cast as

$$I(q) = A\Gamma(D+1)\sin[(D-1) \times \arctan(q\xi)]/(1+q^2\xi^2)^{(D-1)/2}(D-1)q\xi, \quad (1)$$

where $\Gamma(x)$ is the gamma function and A is a parameter given by [21]

$$A \propto \rho_\xi^2 \xi^3 \quad (2)$$

in the case of a mass fractal for which the structure density ρ_ξ scales in a power law with ξ as [22, 23]

$$\rho_\xi = \rho_s(\xi/a)^{D-3}, \quad (3)$$

where ρ_s is the density of the primary silica particles. From equations (2) and (3), we can state that

$$A \propto \xi^{2D-3}. \quad (4)$$

Figure 1 shows the fittings of equation (1) to the experimental SAXS data, using a nonlinear least squares iteration routine (Levenberg–Marquardt algorithm). Table 1 shows the structural parameters A, D, and ξ from the fitting process. The characteristic length ξ increases from ∼1.8 to ∼5.4 nm while the mass fractal dimension D diminishes discretely from ∼2.6 to ∼2.3 as the porosity increases in the range studied. The qualitative appearance of the set of curves of SAXS (figure 1) and the narrow set of values found for the parameter D suggest that all samples are fairly mutually self-similar.

There is no unequivocal crossover at high q in the SAXS curves in figure 1 accounting for the characteristic length a of the primary silica particles building up the mass fractal structure. It should be emphasized that the parameter a could not be obtained by fitting equation (1), since the approach due to Vacher *et al* [21] is valid just for low and intermediate q regions for systems with very small particle size a, so a^{-1} should be greater than the experimental q_{max}. A clearer power law decay $I(q) \sim q^{-D}$ has been observed for analogous TEOS-derived wet sonogels [24] up to a maximum experimental $q_{max} = 4.5\ nm^{-1}$, a value significantly greater than that of the present work. This would imply a characteristic length a smaller than about $1/q_{max} \sim 0.2$ nm. Time-resolved SAXS measurements performed during the formation of TEOS-derived silica gels with an additive [25] also suggest the formation of fractal-like structures from primary units of characteristic length apparently as small as 0.1 nm.

Although a power law with long scaling range could not be unequivocally inferred from the curves in figure 1, the application of the approach of equation (1) is justified on the basis of the ideas from the paper by Avnir *et al* [26], in which there is analyzed the short scaling range that spans only 0.5 to 2.0 decades (factors of 10) with experimentally derived scaling exponents that led to the labeling of the systems studied as fractal. It was concluded that the benefits of describing power law objects as fractal, even for a limited range, outweigh the issue of the perhaps erroneous fractal label. The usefulness is mainly associated with the fact that the power law condenses the description of an often complex geometry and its proportion gives a simple way to correlate properties of a system with its structure and its dynamics of formation. The fractal geometry provides an appropriate language and symbolism for ill-defined geometries [26]. The ability to fit data with a power law over a limited range does not imply fractality, but the fractal label is not really needed [26]. The main point here is that the structure of these systems has a simple description in terms of a two-parameter pair correlation function given by $\gamma(r) \sim r^{D-3}\exp(-r/\xi)$ [20], which is a power law limited by the cut-off distance ξ at large r, in spite of the lack of more information about the small scale cut-off distance a. However, since the sense of self-similarity in irregular objects is comprehended visually even for a limited range of the power law, and since the terminology seems to be deeply rooted in practice [26], we simply will label the present system a 'fractal' for further consideration.

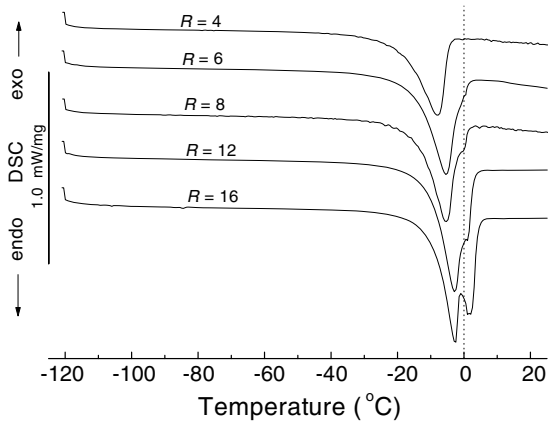

Figure 2. DSC thermograms for pure-water-exchanged wet gels obtained for a heating rate of 2 °C min^{-1}.

Figure 2 shows DSC thermograms obtained at a heating rate of 2 °C min^{-1} for the water-exchanged wet gels previously cooled to −120 °C. The DSC thermogram displays a broad endothermal peak below the normal water melting point, which is associated with the melting of ice nanocrystals. A second sharp endothermal peak with onset temperature close to 0 °C starts to arise as the porosity increases. The latter was associated with the melting of ice macrocrystals.

Neffati and Rault [15] have shown that for a heating rate of 2 °C min^{-1} or slower the DSC thermogram approaches that for the equilibrium conditions for fusion of ice nanocrystals confined in the gels, yielding true information on the 'porous' structure. Under conditions close to the equilibrium, the instantaneous DSC energy flux is proportional to the incremental volume dV of the crystals (or 'pores') melting at temperature T_m. Figure 3 shows the incremental 'pore' volume

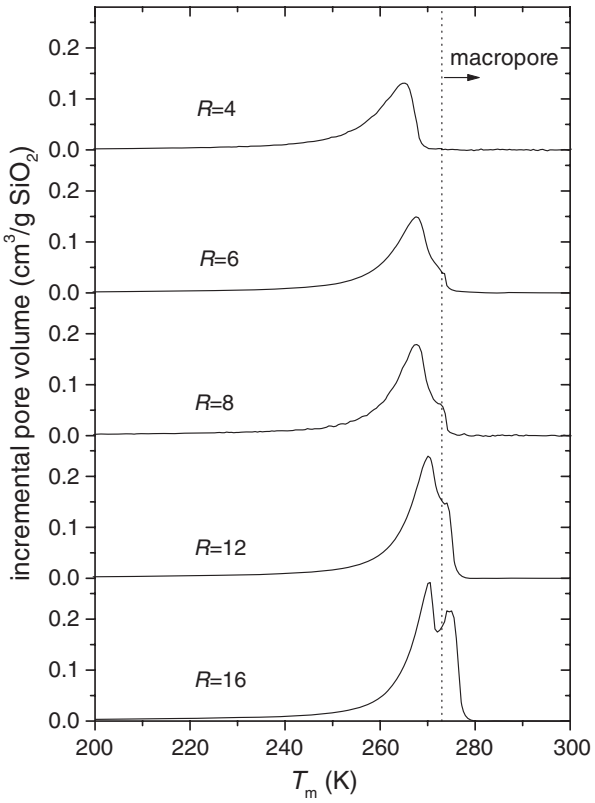

Figure 3. Incremental 'pore' volume per silica mass unit as a function of the melting temperature of the ice nanocrystals.

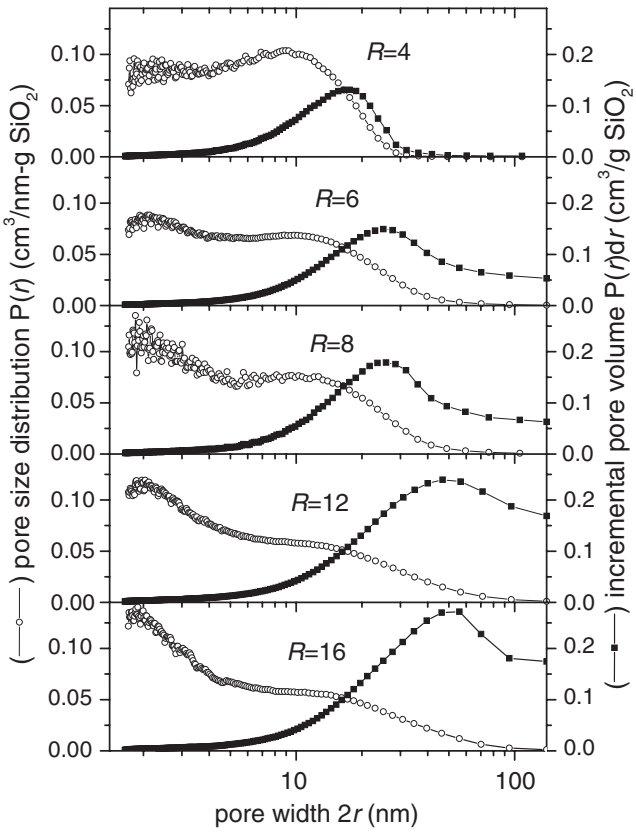

Figure 4. Pore size distribution and the incremental pore volume per silica mass unit as a function of the pore width $2r$.

$\mathrm{d}V$ as a function of the melting temperature as obtained by normalization of the DSC signal with the total pore volume V_p from TG. The macropore volume V_macro in table 1 was obtained by integration of the curves in figure 3 over the range $T_\mathrm{m} \geqslant 273$ K.

According to the Gibbs–Thomson equation, the melting depression temperature $\Delta T_\mathrm{m} = T_\mathrm{m} - T_\mathrm{m}^0$ of an ice nanocrystal with radius r can be evaluated from [15, 27]

$$T_\mathrm{m} = T_\mathrm{m}^0(1 - 2\gamma V_\mathrm{s}/\Delta H r), \tag{5}$$

where T_m^0 is the melting temperature of an ice crystal of infinite dimension, γ the average interfacial tension of the crystal, ΔH the specific melting heat, and V_s the solid specific volume. The Gibbs–Thomson equation applies to cylindrical pores in the case of liquid confined in porous solid [27], by analogy with the Kelvin equation for gas condensation in capillary pores. The crystal–substrate and liquid–substrate interaction terms may be represented as an additional $\cos\phi$ term in the Gibbs–Thomson equation, where ϕ is the wetting or contact angle, commonly assumed to be $-180°$ in the Gibbs–Thomson equation and $0°$ in the Kelvin equation [27]. Then, this $\cos\phi$ term also has a straightforward geometric interpretation since a spherical meniscus of radius R_o, in a cylindrical capillary of radius r, with an angle of contact ϕ, has $r = R_\mathrm{o}\cos\phi$ [27]. In general, the influence of the pore geometry could be taken into account by changing the value of the numerical constant '2' in equation (5) [27].

Assuming for water [15] $T_\mathrm{m}^0 = 273$ K, $\gamma = 40\times10^{-3}$ N m^{-1}, $\Delta H = 334$ J g^{-1} and $V_\mathrm{s} = 1.02$ cm^3 g^{-1}, the introduction of these values in equation (5) yields $T_\mathrm{m} = T_\mathrm{m}^0(1 - 0.25/r)$, where r is given in nanometers. This numerical relation was found to be well applied in the case of a high porosity wet sonogel studied elsewhere [16]. There, the value of the pore size (20 nm) for which there occurred the maximum of the DSC nanocrystal melting temperature peak ($-6.8\,°$C) was found to be in good agreement with the pore size (20 nm) of the maximum in the pore size distribution as determined from nitrogen adsorption, in the corresponding aerogel. Thus, it will be used for further analysis of the pore size distribution of the present sonogels.

The incremental volume of pores with radius between r and $r + \mathrm{d}r$ is $\mathrm{d}V = P(r)\,\mathrm{d}r$, where

$$P(r) = \frac{\mathrm{d}V}{\mathrm{d}r} = \frac{\mathrm{d}V}{\mathrm{d}T_\mathrm{m}}\frac{\mathrm{d}T_\mathrm{m}}{\mathrm{d}r} = \frac{\mathrm{d}V}{\mathrm{d}T_\mathrm{m}}\frac{0.25T_\mathrm{m}^0}{r^2}. \tag{6}$$

Figure 4 shows the pore size distribution $P(r)$ and the incremental pore volume $\mathrm{d}V = P(r)\mathrm{d}r$ as a function of the pore diameter $2r$ for the wet gels.

4. Discussion

The increase of the porosity shifts the mesopore size distribution towards the greater pores, and leads to the appearance of a minor quantity of macroporosity, the macropore volume increasing with the total pore volume. A microporosity is also apparent in all the wet gels in figure 4,

Table 2. Mass fractal characteristics of the wet gel as deduced from DSC pore size distribution.

R	D	$2r_\xi$ (nm)	ρ_{meso} (g-SiO_2/cm^3)
4	2.28 ± 0.07	21 ± 2	0.46 ± 0.01
6	2.39 ± 0.05	32 ± 2	0.44 ± 0.01
8	2.38 ± 0.05	34 ± 3	0.40 ± 0.01
12	2.46 ± 0.04	49 ± 4	0.37 ± 0.01
16	2.47 ± 0.04	52 ± 4	0.36 ± 0.01

although the errors associated with the micropores are critical due to the difficulty of exact subtraction of the baseline in the DSC thermograms in the micropore region. An additional difficulty in characterizing micropores using DSC is associated with the fact that water confined in very small pores does not crystallize completely, since an interface layer of thickness of the order of 0.5 nm remains liquid [28]. Thus water does not crystallize when the dimension of the confinement is less than a critical length equal to ~1 nm.

The DSC mesopore structure could be associated with the mass fractal structure as determined from small-angle x-ray scattering. As the porosity increases the mesopore structure extends towards the greater pore region, increasing the characteristic length ξ and diminishing slightly the fractal dimension D.

The DSC mesopore structure and the SAXS mass fractal characteristics were compared by using an earlier proposed method [29], employed originally to compare SAXS and nitrogen adsorption data in characterizing silica aerogels. We start from a homogeneous solid with the silica density ρ_s (assumed as equal to 2.2 g cm^{-3}) and follow with incorporation into the structure the incremental pore volume per silica unit mass $dV = P(r)dr$ to probe the resulting bulk density $\rho(r)$. The process can be cast as

$$\frac{1}{\rho(r)} = \frac{1}{\rho_S} + \int_0^r P(r)\,dr. \tag{7}$$

The resulting bulk density $\rho(r)$ was assumed as the local density (as probed using the pore width $2r$), which should scale with r in the fractal range $a \leqslant r \leqslant \xi$ as [22]

$$\rho(r) = \rho_S (r/a)^{D-3}. \tag{8}$$

A plot on a log–log scale of $\rho(r)$ as a function of r should be a straight line with slope $D - 3$.

Figure 5 shows the plots of $\rho(r)$ on a log–log scale with the structure length scale, as probed using the pore width $2r$, as evaluated through equation (7) from the pore size distribution $P(r)$ in figure 4. A reasonable fitting of equation (8) to the experimental $\rho(r)$ is observed in the mesopore region, below about a maximum mesopore size, let us say, $2r_\xi$. In the micropore region there is a departure from the linear fitting, mainly for the gels with low porosity. Table 2 shows the mass fractal dimension D and the maximum $2r_\xi$ obtained from the fitting process as a function of the porosity.

The values for D were found all in reasonable agreement with the values determined from SAXS in table 1, although they were found here discretely increasing with the pore volume, instead of decreasing as there.

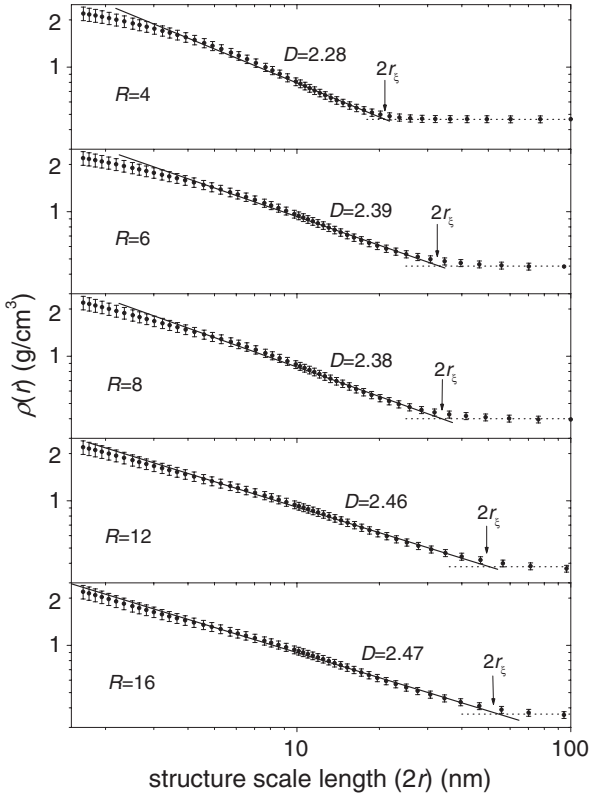

Figure 5. Mass fractal characteristics of the wet gels as deduced from the DSC pore size distribution.

The meaning of the characteristic length ξ in equation (1) is only qualitative and needs to be made more precise in a particular situation [20]. In practice, it can represent the size of an aggregate or a correlation length in a disordered material. For instance, for an isolated mass fractal aggregate of radius of gyration R_g scattering independently, $\xi = [2/D(D + 1)]^{1/2} R_g$ [20]. Using the typical value $D = 2.4$ of the present work, the diameter $D_o = (20/3)^{1/2} R_g$ of an equivalent spherical aggregate would be $D_o \sim 5.2\xi$. For a network fractal structure as adopted in the present work, the meaning of ξ is less intuitive with respect to the size of the fractal structure, but it should be more properly associated with the Bragg distance $2\pi\xi$, as the resolution frequently adopted in the SAXS literature [30]. It should be noted that $D_o \sim 5.2\xi$ for the hypothetical spherical aggregate, of the same order of magnitude as the Bragg distance $2\pi\xi$. Thus, the length scale probed using the pore width $2r$ in building the local function $\rho(r)$ could be properly associated with the Bragg distance $2\pi/q$ in probing the structure using SAXS.

Figure 6 shows SAXS and DSC data as a function of the structure length scale as probed using the pore width $2r$, in the case of DSC, and the Bragg distance $2\pi/q$, in the case of SAXS. There are reasonable correlations between the fractality range and the fractal dimension as probed by the two techniques, inclusive of the departure from the mass fractal characteristics in the micropore region, or at high q.

An independent method for probing the fairly mutual self-similarity of the samples is analyzing the behavior of the SAXS intensity at $q = 0$, which could be done through the parameter

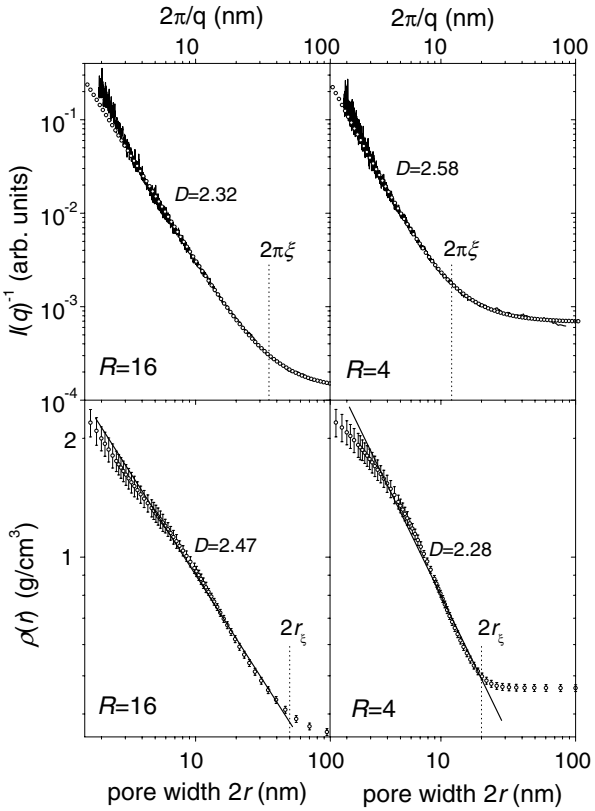

Figure 6. Correlations between the mass fractal characteristics of the wet gels as determined using SAXS and as deduced from DSC. The structure length scale has been probed using the pore width $2r$ in the case of DSC and the Bragg distance $2\pi/q$ in the case of SAXS. The SAXS data were plotted as a $I(q)^{-1}$ versus $2\pi/q$ plot in order to provide a direct view in the real space to compare with the structure length scale $2r$. The small circles are plots of the fitting of equation (1).

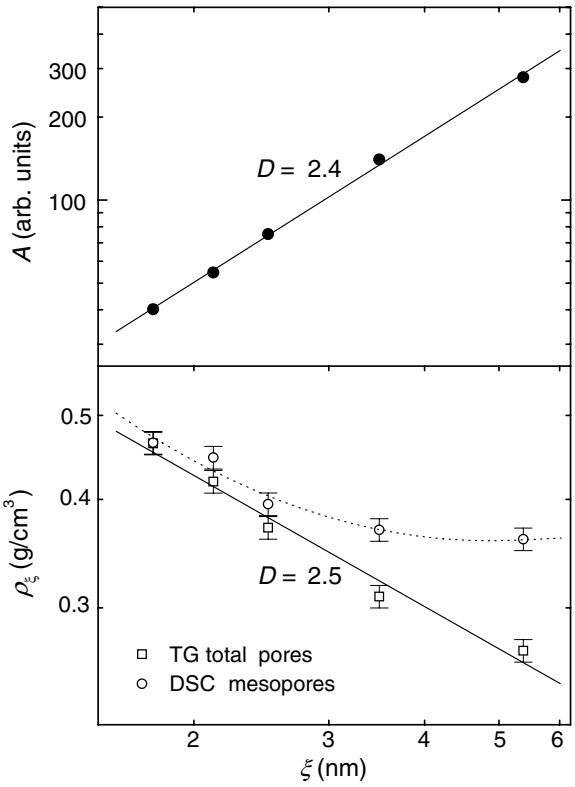

Figure 7. Scaling properties of the wet gels as probed with the intensity power law $A \sim \xi^{2D-3}$ and with the structure density $\rho_\xi \sim \xi^{D-3}$.

A of equation (1). Equation (4) states $A \sim \xi^{2D-3}$, so a plot of A versus ξ on a log–log scale should be linear with slope equal to $2D-3$. Figure 7 (top) shows such a plot and from the slope $2D-3$ we obtain by linear fitting the value $D = 2.4$, which is in reasonable agreement with the typical range of values for D in table 1.

In addition, equation (3) states that the density of the fractal structure ρ_ξ scales in a power law in ξ as $\rho_\xi \sim \xi^{D-3}$. Figure 7 (bottom) shows the plot of the TG-evaluated 'aerogel' density ρ (table 1), assigned here as the fractal structure density ρ_ξ, versus ξ on a log–log scale. From the slope being equal to $D-3$, we obtain the value $D = 2.5$ by linear fitting, which is also in reasonable agreement with the typical values for D in tables 1 and 2.

However, the results are somewhat different if we assign the fractal structure density ρ_ξ to the DSC mesopore-evaluated density ρ_{meso} (table 2), which accounts for the total DSC mesopore volume exclusively. Figure 7 (bottom) shows the plot of ρ_{meso} versus ξ. Clearly the plot departs from linearity for the samples with high porosity. This suggests that the DSC results could be causing misinterpretation of a fraction of mesopores which would be being taken as macropores in the samples with high porosity. This could be due to the fact that water in regions with great mesopores, in which the silica network is very feeble, may not be really confined, so the crystallization of water in such a region would take place as in a unique macropore region. It could also be thought of as a solute rejection mechanism of silica in the freezing of water in such a region of very feeble silica network. Apparently, most of the macroporosity is misinterpreted using DSC for the samples with high porosity. This could be why we have found values for D increasing with the porosity from the DSC pore size distribution (figure 4) instead of diminishing as expected according to the SAXS data.

In a previous work [16] using SAXS, DSC and nitrogen adsorption in characterizing a very high porosity wet sonogel and its so-derived aerogel, we have argued on the basis of the results of Scherer and co-workers [31, 32], that nitrogen adsorption leads one to underestimate significantly the porosity in high porosity aerogels, due to most of the solid surface in aerogels having positive curvature, which does not favor nitrogen condensation, with a consequent underestimation of the porosity. The PSD of the aerogel as determined by the nitrogen adsorption method was found to be in qualitative agreement with the PSD obtained by DSC for the original wet gel [16]. Thus, there may be a certain correspondence between the porosity underestimation resulting from the nitrogen method for aerogels and the porosity underestimation resulting from DSC for wet gels, although the origins are of completely different physical nature.

5. Conclusions

Wet silica sonogels prepared from sono-hydrolysis of TEOS with water/TEOS molar ratio (R) ranging from 4 to 16 present 'porosities' changing correspondingly from 1.70 to 3.28 $cm^3/g\text{-}SiO_2$, after ageing in sealed conditions.

The porosity is composed essentially of nanopores with a pore size distribution which is shifted towards the greater pore region as R increases. A minor fraction of macropores are apparent from the DSC signal, increasing with the porosity. The DSC results could be causing misinterpretation of the macroporosity due to water possibly not being exactly confined in very feeble silica network regions in sonogels with high porosity.

The silica network structure of the wet gels can be described fairly well as mutually self-similar mass fractal structures with correlation length ξ increasing from ∼1.8 to ∼5.4 nm and mass fractal dimension D diminishing from ∼2.6 to ∼2.3, as the porosity increases in the range studied. More specifically, such a structure could be described using a two-parameter correlation function $\gamma(r) \sim r^{D-3}\exp(-r/\xi)$, which is limited at larger scale by the cut-off distance ξ but no well-defined small scale cut-off distance, at least up to the maximum angular domain probed using SAXS in the present study.

Acknowledgments

This research was partially supported by LNLS—National Synchrotron Light Laboratory, FAPESP and CNPq. We thank T Plivelic (LNLS) for his support during the SAXS measurements.

References

[1] Brinker C J and Scherer G W 1990 *Sol–Gel Science: The Physics and Chemistry of Sol–Gel Processing* (San Diego, CA: Academic)
[2] Morita M, Kajiyama S, Rau D, Sakurai T and Iwamura M 2003 *J. Lumin.* **102/103** 608
[3] Sujatha Devi P and Ganguli D 2004 *J. Non-Cryst. Solids* **336** 128
[4] Litrán R, Ramírez-del-Solar M and Blanco E 2003 *J. Non-Cryst. Solids* **318** 49
[5] Litrán R, Blanco E and Ramírez-del-Solar M 2004 *J. Non-Cryst. Solids* **333** 327
[6] Parvathy Rao A and Venkateswara Rao A 2003 *Sci. Technol. Adv. Mater.* **4** 121
[7] Chen W, Zhang J and Cai W 2003 *Scr. Mater.* **48** 1061
[8] Feng Y, Yao R and Zhang L 2004 *Physica* B **350** 348
[9] Ahola M, Kortesuo P, Kangasnieme I, Kiesvaara J and Yli-Urpo A 2000 *Int. J. Pharm.* **195** 219
[10] Radin S, El-Bassyouni G, Vresilovic E J, Schepers E and Ducheyne P 2005 *Biomaterials* **26** 1043
[11] Colomer M T and Anderson M A 2001 *J. Non-Cryst. Solids* **290** 93
[12] Devreux F, Boilot J P, Chaput F and Sapoval B 1990 *Phys. Rev. Lett.* **65** 614
[13] Strange J H, Rahman M and Smith E G 1993 *Phys. Rev. Lett.* **71** 3589
[14] Salvado I M M, Margaça F M A and Teixeira J 1994 *J. Sol–Gel Sci. Technol.* **2** 289
[15] Neffati R and Rault J 2001 *Eur. Phys. J.* B **21** 205
[16] Vollet D R, Donatti D A, Ibañez Ruiz A and Gatto F R 2006 *Phys. Rev.* B **74** 024208
[17] Kellermann G, Vicentin F, Tamura E, Rocha M, Tolentino H, Barbosa A, Craievich A and Torriani I 1997 *J. Appl. Crystallogr.* **30** 880
[18] Schaefer D W and Keefer K D 1984 *Phys. Rev. Lett.* **53** 1383
[19] Freltoft T, Kjems J K and Sinha S K 1986 *Phys. Rev.* B **33** 269
[20] Teixeira J 1988 *J. Appl. Crystallogr.* **21** 781
[21] Vacher R, Woignier T, Pelous J and Courtens E 1988 *Phys. Rev.* B **37** 6500
[22] Zarzycki J 1990 *J. Non-Cryst. Solids* **121** 110
[23] Woignier T, Phalippou J, Vacher R, Pelous J and Courtens E 1990 *J. Non-Cryst. Solids* **121** 198
[24] Vollet D R, Donatti D A and Ibañez Ruiz A 2001 *J. Non-Cryst. Solids* **288** 81
[25] Gommes C, Blacher S, Goderis B, Pirard R, Heinrichs B, Alié C and Pirard J P 2004 *J. Phys. Chem.* B **108** 8983
[26] Avnir D, Biham O, Lidar D and Malcai O 1998 *Science* **279** 39
[27] Webber B and Dore J 2004 *J. Phys.: Condens. Matter* **16** S5449
[28] Rault J, Neffati R and Judeinstein P 2003 *Eur. Phys. J.* B **36** 627
[29] Vollet D R, Donatti D A and Ibañez Ruiz A 2004 *Phys. Rev.* B **69** 064202
[30] Glatter O and Kratky O 1982 *Small Angle X-ray Scattering* (London: Academic) p 136
[31] Scherer G W 1998 *J. Colloid Interface Sci.* **202** 399
[32] Reichenauer G and Scherer G W 2001 *J. Colloid Interface Sci.* **236** 385